JOURNAL OF MATERIALS SCIENCE 5 (1970) 314–325

The Strength and Oxidation of Reaction-Sintered Silicon Nitride

A. G. EVANS, R. W. DAVIDGE
Materials Development Division, AERE, Harwell, Didcot, Berks, UK

The structure of reaction-sintered silicon nitride is studied using scanning electron and optical microscopy at various stages during nitriding, for a range of nitriding and compacting conditions. The strength is then evaluated and interpreted in terms of the microstructure. It is found that fracture always occurs in a brittle manner by the extension of the largest pores. The effects of prolonged annealing in air above 1000° C on both the structure and strength are investigated. At 1400° C, cristobalite is formed. If the temperature is then maintained above 250° C, the strength is enhanced, but below this temperature the oxide layer cracks and reduces the strength.

1. Introduction

There is an increasing awareness that silicon nitride is an outstanding ceramic material for consideration in high temperature engineering applications [1-3]. Metals generally suffer from creep and/or oxidation problems at temperatures $> 1000°$ C and the question naturally arises as to whether ceramics – with their good high temperature strength and oxidation resistance – could be used instead. The attractiveness of silicon nitride depends to a large extent on its very low coefficient of thermal expansion, relative to other ceramics, which leads to a good thermal shock resistance. The use of silicon nitride as a structural component presents many difficulties. On the engineering side the problems are associated mainly with brittleness under tensile stresses, with the attendant notch sensitivity and susceptibility to catastrophic failure on impact conditions. With suitable design philosophy and by subjecting components primarily to compressive stresses many of these problems can be solved. On the materials science side the problems lie in determining the factors controlling the high temperature properties of silicon nitride, particularly tensile strength and oxidation resistance: this is the concern of the present paper.

Most silicon nitride is made by a reaction-bonding process which involves heating compacted silicon in a nitrogen atmosphere. Firing is usually conducted in two stages: the first below the melting point of silicon (1400° C) and the second above the melting point. A typical firing schedule would be 1350° C for 24 h plus 1450° C for 24 h. Below the melting point of silicon, interlocking acicular growths of Si_3N_4 form between the silicon particles by a vapour transfer mechanism [1]. When an interconnecting skeleton has formed, the temperature can be raised above the melting point of silicon, where the reaction occurs more rapidly to form granular Si_3N_4. It is generally considered that the acicular phase is α-Si_3N_4 (actually an oxynitride of approximate composition $Si_{11.5}N_{15}O_{0.5}$ [4]) and that the granular phase is a mixture of α- and β-Si_3N_4 [5, 6]. The production of α-Si_3N_4, relative to that of β-Si_3N_4, is favoured by high oxygen potentials and low temperatures. On thermodynamic grounds it is very difficult to suppress the formation of α-Si_3N_4 – an oxygen potential of $< 10^{-19}$ atm would be required at 1400° C [4]. However, the thermodynamic factors are not generally decisive so that most materials comprise a mixture of α- and β-Si_3N_4. In addition, an α to β transition can occur at $\sim$ 1600° C although this does not appear to be reversible [7]. There is very little volume change during nitriding, $< 0.1\%$, so there is an increase in density; the maximum density that can be attained by reaction bonding is $\sim 2.7\ 10^3$ kg m^{-3} (theoretical density: $3.2\ 10^3$ kg m^{-3}).

Several workers [6, 8-11] have measured the strength of silicon nitride. The room temperature strength decreases with decrease in density, from

$\sim$200 MN m^{-2} for a density of 2.6×10^3 kg m^{-3}, to $\sim$100 MN m^{-2} for a density of 2.2×10^3 kg m^{-3}. The temperature-dependence of the strength depends on the source of the material but the strength at 1200° C is usually as high or higher than that at room temperature. There has been little attempt at a correlation between strength and structure. Oxidation resistance is generally described as "good" at 1400° C [2] but detailed effects of oxidation on strength have not been examined.

The objectives of the present work are threefold: to determine the relationship between the structure of the original silicon compact, the nitriding conditions, and the final fired structure; the measurement of the strength and an explanation in terms of structure; and the effect of high temperature oxidation on strength. Reaction bonded material of density 2.5×510^3 kg m^{-3} is used for the bulk of this work but with some data on material of density 2.13×10^3 kg m^{-3}.

2. Experimental

Silicon compacts were made by pressing a commercial grade silicon (98% pure, particle size 10μm, mean, 25μm max.) with an organic binder at pressures < 1 GN m^{-2}. These were nitrided to various schedules in a nitrogen atmosphere containing $\sim$ 2 ppm oxygen.

The fracture stresses were determined in three-point bending using specimens 24 × 5 × 4 mm and a knife edge span of 20 mm. Specimens were machined from discs of material and some were polished. The time to reach the fracture stress was $\sim$ 1 min. Tests in air were conducted in a silicon carbide furnace using silicon nitride knife edges; tests in argon were conducted in a molybdenum furnace, using tungsten knife edges [12].

A discussion of strength in terms of structure requires the evaluation of the effective surface energy for fracture initiation (γ_i), of Young's modulus, and an examination of the flaws in the material. γ_i is determined from three-point bend tests from the stress to extend large artificially introduced flaws [12-15]. In polycrystalline oxides the stress to extend a machined notch is similar to that to extend a sharp crack of similar dimensions [12-15], and tests on bars with machined notches are adequate. In Si_3N_4, however, it is found that the stress to extend a machined notch is about twice that to extend a sharp crack, as in glass or polymethyl methacrylate [13], thus tests must be conducted on bars with sharp cracks. Bars containing sharp cracks are prepared as illustrated in fig. 1. A compressive stress is applied parallel to the plane of a small machined notch in a plate, so that the crack grows from the notch in a controlled manner [16]. The plate is then sectioned to produce two bend specimens. The cracks may be observed optically on a polished face or by using a dye penetrant.

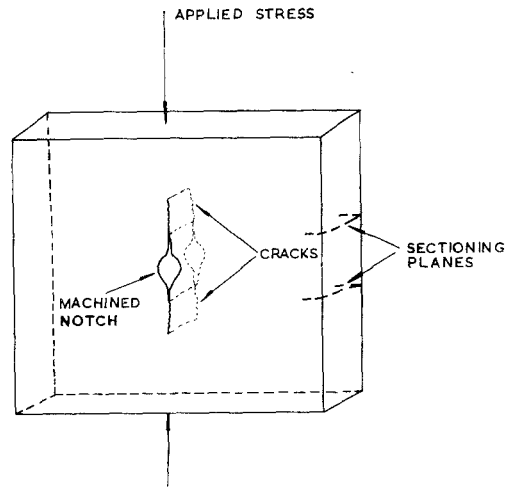

Figure 1 Schematic representation of the method for the production of three-point bend specimens containing sharp-edge cracks.

3. Relationship Between Microstructure and Fabrication Variables

In this section the microstructure of the silicon compacts, and how these change during a range of nitriding schedules, are examined by scanning-electron and optical microscopy. Most of the porosity in reaction-bonded silicon nitride is on a very fine scale (10 to 100 nm diameter). Here we are concerned mainly with the large pores (10 to 50μm diameter) which are expected to control strength.

A typical compact, after the binder has been burnt off, is shown in fig. 2. The silicon particles vary in size from 25 to 3μm, and no significant fracture of the particles occurs during compaction. The size and distribution of the pores depends on the compacting pressure (P), and, the higher the density the smaller the pores. The densities of the green compact and the fully nitrided product are $\propto \log P$, fig. 3.

On nitriding below the melting temperature of silicon, the pores of the silicon compact

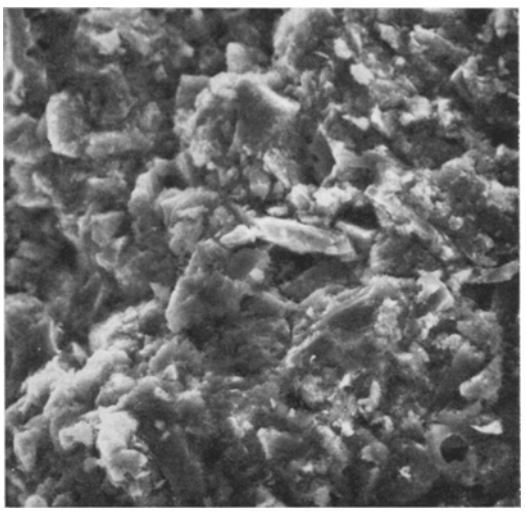

Figure 2 Scanning electron fractograph of a silicon compact with density 1.6 10^3 kg m^{-3} ($\times$ 715).

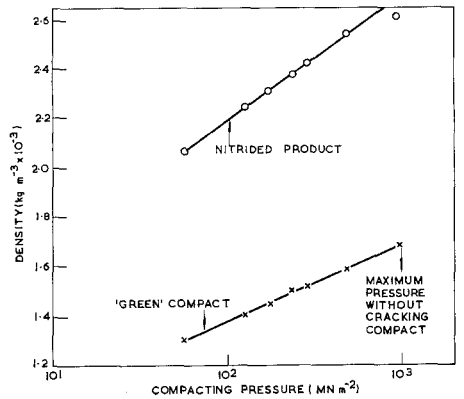

Figure 3 The effect of compacting pressure on the "green" density of the silicon compact and the density of the nitrided product.

start to fill with silicon nitride needles (fig. 4a), and small areas of silicon are converted into granular silicon nitride (fig. 4b). X-ray analysis reveals that most of the silicon nitride is in the α-form, although significant amounts of β are formed at temperatures approaching 1400° C. Thus, at 1350° C for instance, the proportion of silicon nitride in the β-form is $\sim$ 15%, throughout the nitriding operation. Continued sintering increases the density and thickness of the needles so that a matte of silicon nitride gradually replaces the silicon (figs. 4c, d). The nature of the matte after complete nitriding depends on the density of the silicon compact and hence, on the compacting pressure. For low density compacts, the acicular nature of the matte is retained (fig. 4c), so that the sintered product also has a relatively low density. For higher density compacts the matte has a denser appearance (fig. 4d), and the sintered product has a relatively high density. It is probable that the original needles have grown together and lost their identity. However, not all of the pores in the original compact are converted into a matte. Certain of the larger pores are only partially filled with needles (fig. 4e). A histogram of pore-sizes in material nitrided primarily below the melting temperature of the silicon (fig. 5), shows that the pores in the final product are all $\leqslant 16\mu$m in diameter. They are thus similar in size to the largest pores in the original compact.

4(a)

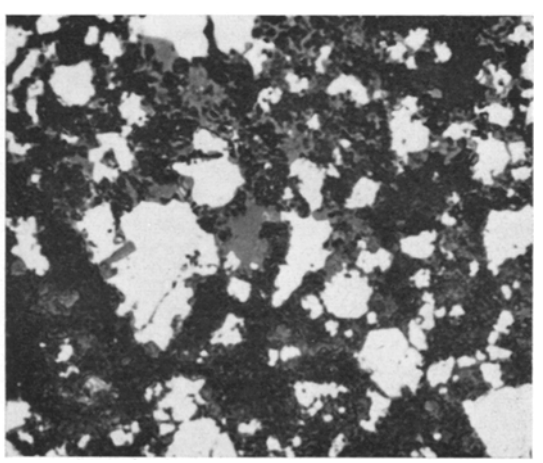

4(b) (cont)

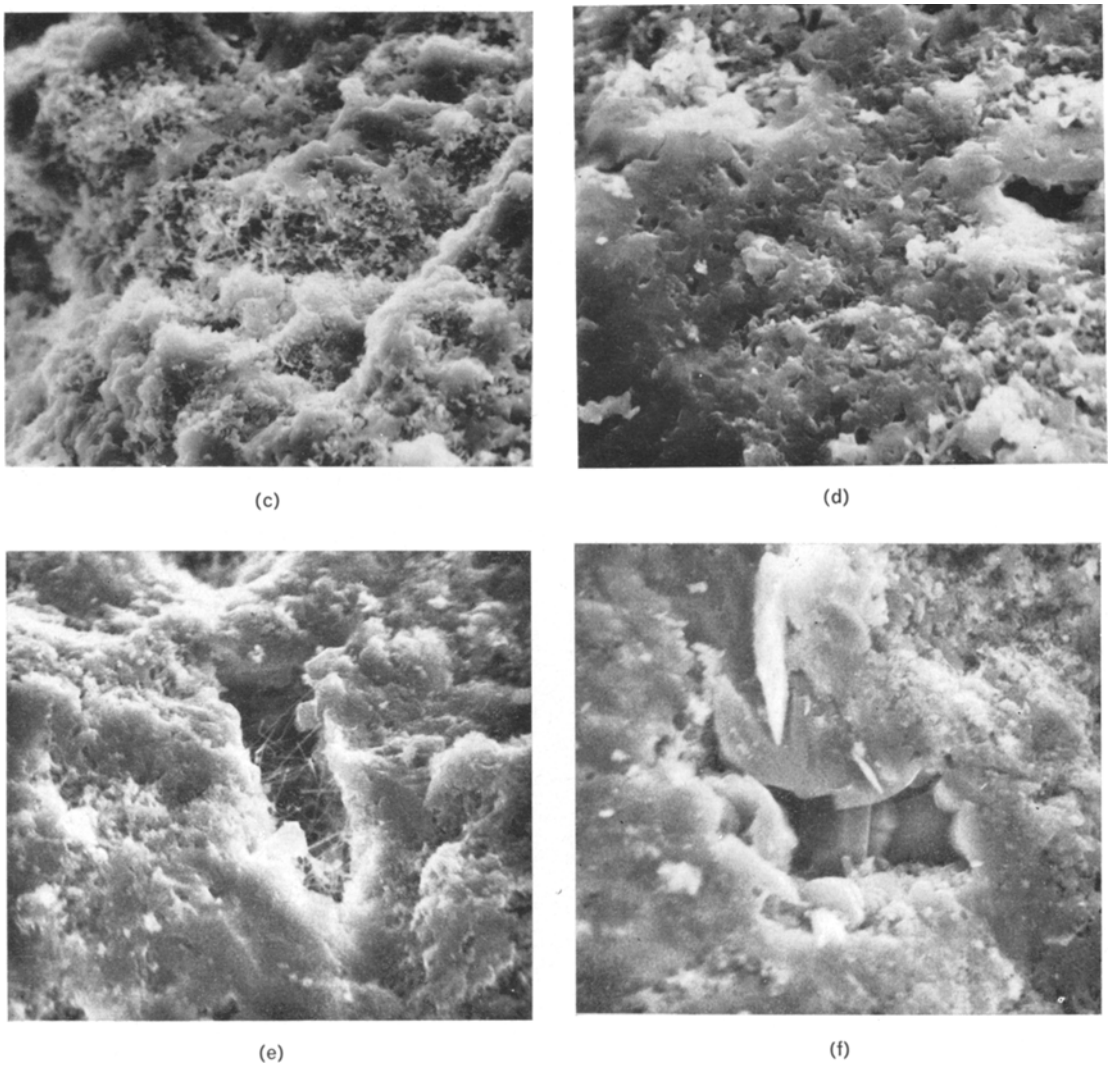

Figure 4 (a) Scanning electron fractograph of a specimen that has been reaction sintered for 1 h at 1350° C (× 1833). (b) Optical micrograph of a polished section through a specimen that has been reaction sintered for 5 h at 1350°C (× 712). The white areas are silicon, the grey silicon nitride and the background is the matte. (c) Scanning electron fractograph of a specimen with a density of 2.13 10^3 kg m^{-3}, nitrided to completion at 1350° C (× 1833). (d) Scanning electron fractograph of a specimen with a density of 2.55 10^3 kg m^{-3}, nitrided to completion at 1350° C (× 4819). (e) Scanning electron fractograph of a specimen (density, 2.55 10^3 kg m^{-3}) nitrided to completion at 1350° C, showing the incomplete matte formation in the largest non-slit-like pores of the original compact (× 2409). (f) Scanning electron fractograph of a specimen (density, 2.55 10^3 kg m^{-3}) nitrided for 5 h at 1350° C and 24 h at 1450° C, showing a pore created when molten silicon runs into the surrounding matte (× 2147).

Sintering below the melting point of silicon tends to completion only after long times, $> 10^3$ h, and to reduce the total sintering time it is convenient to incorporate a second sintering stage above the melting point of silicon. X-ray analysis reveals that most of the silicon nitride formed in this stage is in the β-form. The α/β ratio in the final product is related primarily, therefore, to the proportions of the sintering conducted in the two stages and, to a lesser extent, to the sintering temperature in the first stage. Typically, sintering for 5 h at 1350° C plus 30 h at 1450° C gives a product with $\sim 25\%$ α, whilst sintering for 150 h at 1350° C

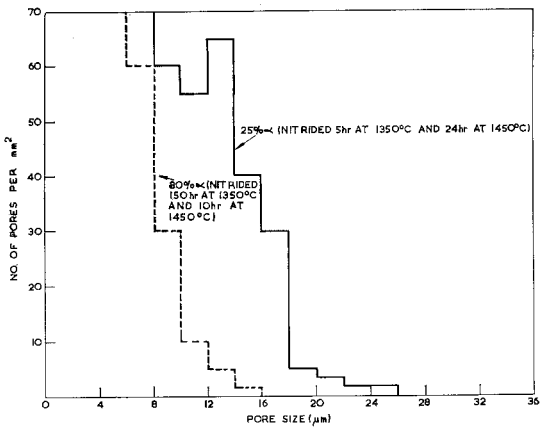

Figure 5 A histogram of large pore-sizes in materials containing 25% and 80% of the α-phase respectively. The former was nitrided primarily above the silicon melting temperature, and the latter mostly below the silicon melting temperature.

plus 10 h at 1450° C gives a product with $\sim 80\% \alpha$.

In material that has been sintered, in part, above the melting temperature of the silicon, large pores of a different type are detected (fig. 4f). They do not contain whiskers and are surrounded by relatively coarse-grained nitride. A histogram of pore-sizes for material nitrided primarily above the melting temperature of silicon (fig. 5), shows that pores up to 26μm in diameter are present. These are larger than the pores in the original compact. They are not formed when the silicon is solid, so their formation requires the presence of molten silicon. Also, the largest of these pores are similar in size to the largest silicon particles. These observations imply that certain silicon particles, when molten, can run into the surrounding matte, leaving behind a large pore. The precise conditions needed for this process are too complex to define at this stage. However, if it can be shown that molten silicon is absorbed by porous silicon nitride, then it is reasonable to consider that the pores will form where the molten silicon is not surrounded by an effective retaining "skin" of nitride. An experiment designed to determine whether molten silicon can run into a matte of silicon nitride is described below.

Firstly, silicon is melted in a crucible in an argon atmosphere and a silicon nitride specimen allowed to float on the surface: it is found that the silicon tends to penetrate the nitride (fig. 6a).

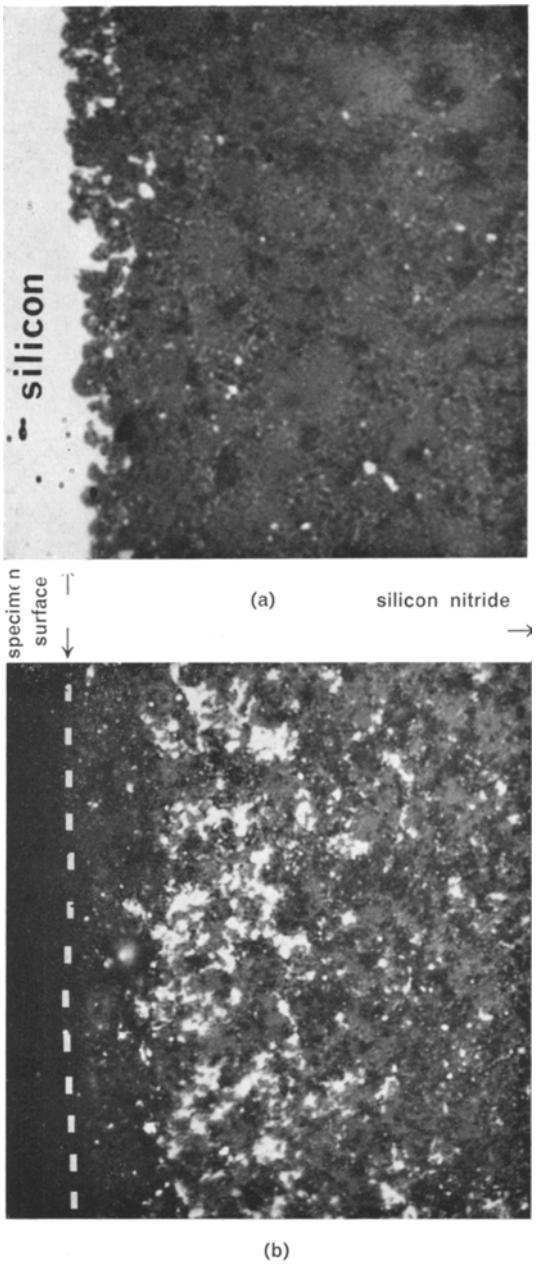

Figure 6 (a) Optical micrograph showing the penetration of silicon into silicon nitride when the nitride is floated in molten silicon; the white areas are the silicon (× 1540). (b) Optical micrograph showing the penetration of the silicon nitride when the silicon is remelted (× 1540). Note that the band adjacent to the surface which contained the silicon in (a) is now free of silicon.

The silicon, other than that which has been absorbed, is then carefully removed by grinding, and the specimen reheated in argon to melt the re-

maining silicon – with the face containing the absorbed silicon on top. It is found that the silicon penetrates quite deeply into the nitride (fig. 6b) and must have run from the suface pores through the surrounding matte, leaving the surface relatively free of silicon. This is analogous to the effects that could occur if the molten silicon is not retained by a "skin" of nitride during the nitriding process.

In a typical nitrided body, therefore, there will be two types of pore: those present in the original compact, and, those formed when large silicon particles melt and are absorbed by the matte. The first type of pore depends on the silicon particle packing in the green compact: slit-like defects may be bridged by α-Si_3N_4 whiskers, but the large, more spherical defects will remain. The second type of pore is determined by the size of the silicon particles at the end of the first stage of nitriding and can be suppressed by nitriding for long times below the melting point of silicon.

The size of the largest pores may thus depend upon the nitriding schedule if the silicon particles are larger than the pores in the silicon compact. This is amply demonstrated in fig. 5 for material of density 2.55 10^3 kg m^{-3}. Alternatively, in material of density 2.13 10^3 kg m^{-3} the largest pores in the green compact are $\sim 50\mu m$ in diameter, which is greater than the size of the largest silicon particles. In this case the pores in the nitrided material do not depend critically on the nitriding schedule and are always $\sim 50\mu m$ in diameter.

In general, therefore, a small final pore-size will be favoured by high green density, small silicon particle-size, and nitriding schedules which are predominantly below the melting point of silicon.

4. The Strength of Silicon Nitride

In this section, the effects of the fabrication variables and temperature on the strength of silicon nitride are studied, to relate the strength to microstructure. Fracture-initiating mechanisms are identified by evaluating the stresses to extend the inherent flaws and the stresses for crack-initiation by plastic flow. Effects of high temperature oxidation on strength are considered later in section 5.

4.1. Fracture Strength

Fig. 7 shows strength at 20° C as a function of the proportions of α- and β-Si_3N_4, for material

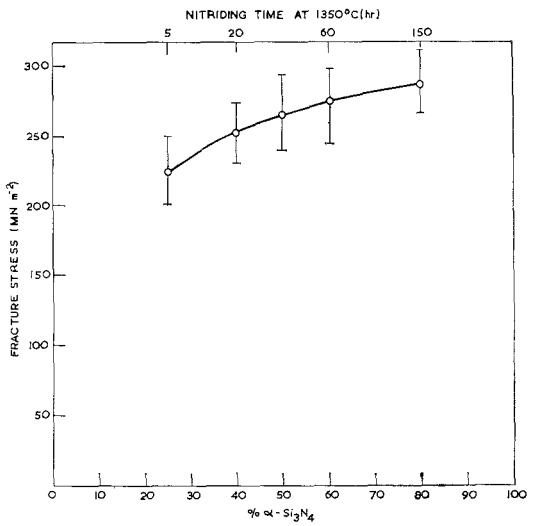

Figure 7 The fracture stress of silicon nitride at room temperature, as a function of the α/β ratio. Nitriding is conducted initially at 1300 to 1350° C (the times at 1350° C are indicated on the diagram) and completed at 1450° C where necessary. The error bars indicate the standard deviation.

fired to different schedules at 1350° C plus 1450° C. The strength increases with increasing proportion of α-Si_3N_4, but the effect is small for α contents $\geqslant 60\%$. Because long nitriding times are required to produce large proportions of α-Si_3N_4, the subsequent work is on material containing 60% α-Si_3N_4.

The effect of temperature on the strength, for material of two densities, tested in purified argon, is shown in fig. 8; the strengths are similar for machined and polished surfaces. The load-deflection curves do not deviate from linearity prior to fracture, even at 1800° C where the material begins to sublime. There is thus no gross plasticity before fracture in this material, at the strain-rate used. There is a strong variation of strength with the density, but only a weak dependence on the temperature.

4.2. The Fracture Mechanisms

The framework for the interpretation of the strength of brittle materials has been described elsewhere [12-15]. According to this framework, fracture occurs by the extension either of inherent flaws or of flaws generated by plastic flow. In the former case, the fracture stress, σ_f, is given quantitatively by:

$$\sigma_f = \frac{1}{Y}\left(\frac{2E\gamma_i}{C}\right)^{\frac{1}{2}} \quad (1)$$

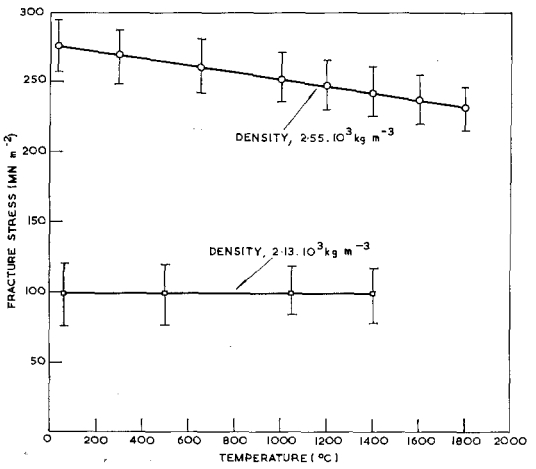

Figure 8 The temperature-dependence of the strength of material of two densities, 2.55 10^3 and 2.13 10^3 kg m^{-3} respectively, tested in a purified argon atmosphere.

where E is Young's modulus, C is the size of the largest inherent surface flaw, γ_i is the effective surface energy for fracture initiation and Y is a geometrical constant [17]. In the latter case, the fracture stress is related to a flow stress, either the stress for dislocation-initiated cracking [12, 14, 18] or the stress for grain-boundary-sliding-induced cracking. To identify the fracture-initiating mechanism, therefore, it is necessary to evaluate independently the magnitude of the largest inherent flaws and the effective surface energy. The stress to extend these flaws may then be compared with the observed fracture stress. If these are similar, the fracture mechanism is immediately identified. Whereas if the latter is lower, it is likely that fracture is initiated by plastic flow, and it remains to relate the fracture stress to the appropriate flow stress.

Values of E, γ_i and C (see section 3) are thus required for each of the above fabrication conditions and temperatures to enable the stresses to extend the inherent flaws to be evaluated. Also, since valid γ_i values can only be obtained from equation 1 provided that $\sigma_f \leqslant 0.4\sigma_y$ [17], where σ_y is the flow stress, a value of σ_y is needed.

4.3. The Stresses for Plastic Flow

There have been no investigations of dislocation motion in silicon nitride. It is necessary therefore to revert to microhardness measurements to obtain an approximate value for the yield stress [19]. The microhardness of dense Si_3N_4 at room temperature is $\sim$ 25 GN m^{-2}, which indicates a yield stress $\geqslant$ 7 GN m^{-2}. The measured fracture stresses are thus well below the stress for plastic flow within grains, at least at room temperature.

The stresses required for gross plasticity can be obtained from compression tests [12, 18] and a number of tests have thus been conducted, up to 1800° C. No deviations from linearity are encountered prior to fracture in any of the tests. The highest stresses reached are 450 MN m^{-2}; the stresses required for gross plastic flow are in excess of this. The observed fracture stresses are thus much lower than the flow stress so that valid γ_i values may be obtained from equation 1 for all temperatures $<$ 1800° C.

4.4. Young's Modulus

Values of Young's modulus for materials of density 2.55 and 2.13 10^3 kg m^{-3} are shown in fig. 9, and are compared with the latest values obtained by other investigators. The results fit a single curve quite closely. There is a marked decrease in modulus with increase in porosity, whereas the α/β ratio has no significant effect. The effect of temperature has not been investigated, but Lloyd [9] showed that there is a small linear decrease with increase in temperature.

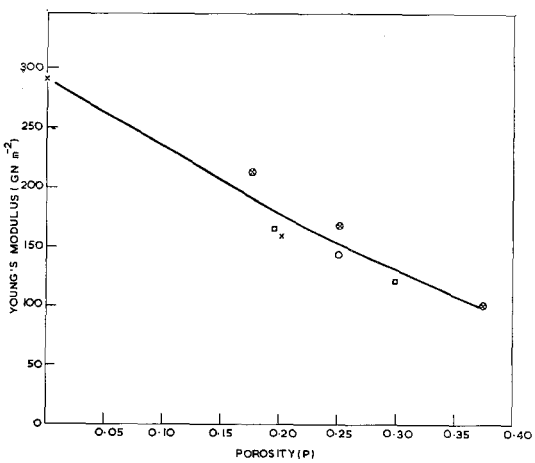

Figure 9 The effect of porosity on Young's modulus. ×, Lloyd [9]; ⊗, Parr and May [1]; ○, Doulton – quoted by Thompson and Pratt [6]; □, current investigation.

4.5. The Effective Surface Energy for Fracture Initiation, γ_i

The values of γ_i obtained from the stress to

extend sharp cracks are shown in table I. $\gamma_i \sim 6$ J m^{-2} for material of density 2.55 10^3 kg m^{-3}. There is no marked variation of γ_i with either α/β ratio or temperature, although γ_i decreases with increase in porosity, to ~ 4 J m^{-2} for material of density 2.13 10^3 kg m^{-3}.

TABLE I The effective surface energy for fracture initiation γ_i.

Material		γ_i, J m^{-2}
Density =		
2.55 10^3 kg m^{-3}	80% α (20° C)	6 ± 2
	25% α (20° C)	6 ± 2
	60% α (20° C)	6 ± 2
	60% α (1450° C)	6 ± 2
Density =		
2.13 10^3 kg m^{-3}	60% α (20° C)	4 ± 1.5

The γ_i values obtained are lower than those for Al_2O_3 [15] and MgO [14, 18], and similar to those for UO_2 [12] and glass [13]. It is likely that plastic flow contributes in part to γ_i, as in most ceramic materials, but the volume of the plastic zone must be small. An approximate value of the radius of the plastic zone at the crack-tip, r, may be obtained from [20]:

$$r = \left(\frac{\sigma_a}{\sigma_y}\right)^2 \frac{C}{2}, \qquad (2)$$

where σ_y is the yield stress and σ_a the applied stress. If the value of σ_y obtained from microhardness is used, a value of $r < 10$ nm is obtained.

The fact that γ_i is relatively independent of the structure, for a given density, is of great importance. This implies that γ_i is not only insensitive to the α/β ratio but also to the size and distribution of pores and perhaps the distribution of grain-sizes. The small decrease obtained on increasing the porosity can be accounted for in simple terms by the reduction in the area of new surface that must be created by the propagating crack.

4.6. The Stresses to Extend the Inherent Flaws

The largest inherent flaws are the pores considered in section 3. The stress to extend these flaws may be obtained from a fracture stress equation similar to equation 1, provided that the appropriate γ_i value is known. The form of the equation depends almost exclusively on the largest dimension of the flaw and the form of the tip. The largest circumference of a pore is approximately circular in shape and contains sharp grooves (figs. 4e, f), so the stress σ_p to extend the pores is given approximately by the stress to extend a sharp penny-shaped flaw with similar diameter [21]:

$$\sigma_p = \left(\frac{\pi E \gamma_i}{2C}\right)^{\frac{1}{2}}. \qquad (3)$$

The appropriate γ_i-value is now required to enable σ_p to be evaluated. The measured values of γ_i (table I) are for edge-cracks ~ 2 mm long. They can be used to evaluate σ_p provided that the shape and size of the plastic zone is the same for the penny-shaped cracks as for the edge-cracks and that γ_i is independent of crack length, C, for cracks between $\sim 10\mu$m and 2 mm in length. The shape of the crack front only has a significant effect on the plastic zone size for large plastic zones. Since the plastic zone size is < 10 nm in this material, the γ_i-values measured for edge-cracks can be applied to penny-shaped cracks. The effect of C on γ_i is more difficult to establish, but the information obtained on other materials has enabled certain criteria to be laid down. In polycrystalline ceramics, it has been found that γ_i depends only on crack length when the plastic zone size is comparable to the crack length. Thus, in MgO where the plastic zone is a few G in length (where G is the grain-size) γ_i does depend on the crack length, but then only for cracks $\leqslant 5G$ [14]. Whereas in Al_2O_3, where the plastic zone size is $< G$, γ_i is independent of C for all cracks $> G$ in length [22]. In Si_3N_4, not only is the plastic zone size $< G$, but $C >$ a few G. The measured values of γ_i for cracks ~ 2 mm in length should thus be suitable for the evaluation of the stress to extend pores $\sim 10\mu$m in diameter.

The stresses, σ_p, to extend the largest flaws determined from equation 3 are given in table II, where they are compared with the measured fracture stresses. The calculated and measured stresses agree within the experimental scatter. It is probable then that fracture occurs by the extension of the largest pores in a brittle manner under all the test conditions.

In summary, the strength of reaction-bonded silicon nitride can be explained in terms of the extension of inherent flaws. For a given material, γ_i varies little with temperature. The effect of temperature on strength is small and is related primarily to the temperature-dependence of

TABLE II Comparison of the fracture stresses with the stresses to extend the largest pores

Material		σ_f, MN m^{-2} (measured)	σ_p, MN m^{-2} (calculated)
Density = 2.55×10^3 kg m^{-3}	80% α (20° C)	285 ± 30	300 ± 100
	25% α (20° C)	220 ± 30	240 ± 80
	60% α (20° C)	275 ± 30	290 ± 100
	60% α (1450° C)	235 ± 30	250 ± 80
Density = 2.13×10^3 kg m^{-3}	60% α (20° C)	100 ± 20	120 ± 40

Young's modulus. For materials of a given density, a variation in the α/β ratio leads to little variation in γ_i, but can give a large variation in the largest flaw size C. Thus for material of density 2.55×10^3 kg m^{-3}, a high α/β ratio leads to the greatest strength, not because of intrinsic differences between the strengths of the two phases, but because of the smaller flaw sizes present. The effect of variations of porosity on strength is more complex because an increase in porosity tends to decrease E and γ_i and increase C, all of which reduce strength.

It is interesting to speculate on the ultimate strength of silicon nitride. Lumby and Coe [23] have obtained strengths of up to 1.0 GN m^{-2} for fully dense hot-pressed material. The mean grain size was 0.3μm but other "structural features" of $\sim$ 3μm diameter were also observed. Assuming that γ_i for dense material is $\sim$ 8 J m^{-2} (i.e. larger than the reaction-sintered material due simply to the higher density) and that these "features" act as flaws, then the strength according to equation 3 is 1.1 GN m^{-2}, in good agreement with the observed value. Clearly if these "features" could be eliminated, a tenfold reduction in flaw size may occur giving strengths of $\sim$ 3 GN m^{-2}.

5. The Oxidation of Silicon Nitride

Some of the uses envisaged for silicon nitride require that it should retain a reasonable strength in oxidising environments at high temperatures. It is of great importance therefore to understand the effects of oxidation on strength. Certain aspects of the oxidation behaviour have thus been studied: the amount of oxide formed has been evaluated by weight gain experiments and by X-ray analysis, and the microstructure of the oxide studied in the scanning electron microscope. Then, the effects of oxidation on strength have been determined. All oxidation experiments were conducted in air.

5.1. Microstructural Aspects

Significant oxidation of silicon nitride occurs at temperatures above 900° C, principally by the formation of silica. On cooling to room temperature, crystalline silica – cristobalite – is detected by X-ray diffraction analysis. After oxidation at 1400° C, a similar quantity of cristobalite is detected on specimens that have been either air-cooled or water-quenched, so it is likely that the oxide is formed as cristobalite at the oxidation temperature. This is consistent with observations that amorphous silica tends to transform to cristobalite above 1200° C ([25], p. 347). Also, all the oxygen weight gain can be accounted for as cristobalite, so that no significant amounts of oxynitride can have formed. For material of density 2.55×10^3 kg m^{-3} and a specimen cross-section 3 × 6 mm, the rate of oxidation at 1400° C is initially very rapid, $\sim$ 4% cristobalite in 10 min. The rate then drops off rapidly so there is still only, $\sim$ 8% cristobalite in 600 h.

Some microstructural features of a specimen oxidised for 72 h at 1400° C (6% cristobalite) are shown in fig. 10a. Microstructural alterations are apparent to a depth of $\sim$ 20μm. Optical examination reveals a discrete dense oxide layer 5μm thick and a sub-surface layer 15μm thick that has been extensively oxidised and contains fine porosity. The oxidised layer is severely cracked, fig. 10b. The cracks penetrate to a depth of $\sim$ 15μm. A 20μm thick oxide layer accounts for $< \frac{1}{4}$ of the total cristobalite present so that the bulk of the oxidation occurs throughout the volume of the specimen, presumably round the pores. This suggests that the initial oxidation rate should be very rapid and then fall drastically once a discrete surface layer has formed.

There is a large volume increase when silicon nitride is converted to silica which may generate compressive stresses in the oxide. If these compressive stresses are large enough the oxide film could buckle and then crack. The cracks observed in the silica surface layer could thus have been created during the formation of the layer at 1400° C. If so, the thicker the layer the

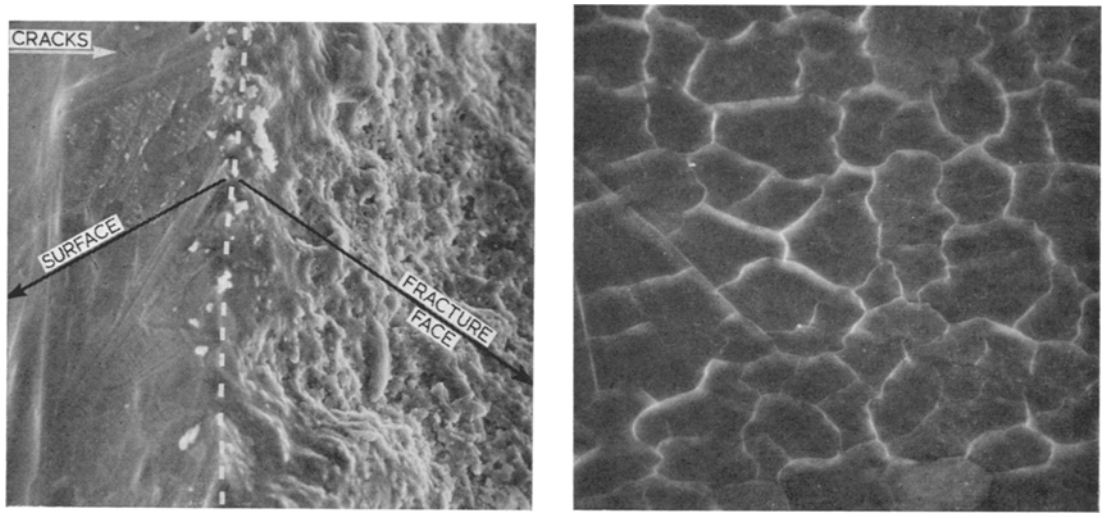

(a) (b)

Figure 10 (a) Scanning electron micrograph of a specimen oxidised for 72 h at 1400° C, taken at the intersection of a fracture face with the oxidised surface (× 960). (b) Scanning electron micrograph of the oxidised surface of the same specimen as in (a) (× 565).

greater the tendency for cracking [24]. Alternatively, the cracks may form on cooling. Although the thermal expansion coefficients of cristobalite and silicon nitride are similar above 250° C (3.0 and 2.5 10^{-6} (deg C)$^{-1}$ respectively), high cristobalite converts to low cristobalite at ~ 250° C with an accompanying 5% decrease in volume. Large tensile stresses are generated in the oxide during this transition which could lead directly to cracking. If cracking occurs in this way, the tendency towards cracking is relatively independent of the thickness of the oxide layer ([25], p. 483).

At 1400° C, it is observed that the oxide layer can be extensively deformed, without any associated cracking, by running a silicon nitride rod over the surface. This plasticity would tend to relieve any stresses generated in the oxide during its formation at this temperature. It is likely then that the cracks in the oxide are created during cooling, rather than during the formation of the oxide.

5.2. The Effects of Oxidation on the Strength

The effects of oxidation depend sensitively on the specimen history. Four types of experiment have been conducted: (a) oxidation at the test temperature; (b) oxidation above 1000° C and then lowering to the test temperature; (c) oxidation above 1000° C followed by cycling to room temperature before testing at the oxidation temperature; (d) oxidation followed by removal of the oxide layer (by grinding) and testing at room temperature. The effects of each of these operations on the strength are considered in turn.

Oxidation at the test temperature, above 1000° C, for up to 1 h, gives a marginal increase in strength, < 10% (fig. 11). At 1400° C, no further increase is observed for oxidations up to 100 h, whereas at 1000° C, the strength continues to increase the longer the oxidation time and reaches 350 MN m^{-2} after 100 h (fig. 11).

More remarkable strength changes are en-

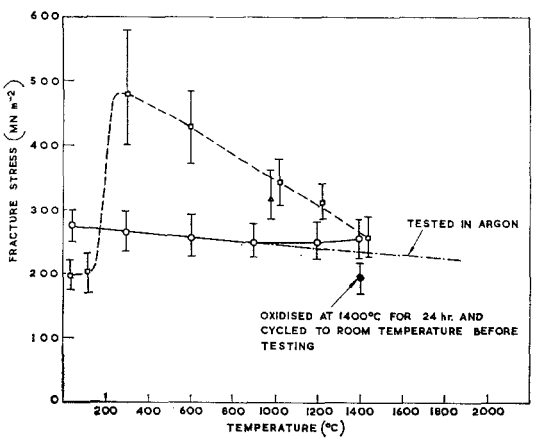

Figure 11 The effects of oxidation on the strength of silicon nitride. ○, annealed at test temperature for 20 min; □, annealed for 24 h at 1400° C and lowered to test temperature; △, annealed for 100 h at test temperature.

countered by oxidising at high temperature and then lowering to the test temperature (fig. 11). For 24 h oxidation at 1400° C, the strength continues to rise quite steeply with decrease in temperature down to ~ 300° C, and reaches almost 500 MN m^{-2}. Then, at lower temperatures there is a sharp drop in strength to 200 MN m^{-2}, i.e. weaker than the unoxidised material. In addition, it is noted that the strength between 300° C and room temperature is dependent on the time that the specimen is held at the test temperature prior to testing. For short times (~ 20 min at 200° C and 2 min at 20° C) the strength is still ~ 500 MN m^{-2}, but for longer times it drops to 200 MN m^{-2}.

Cycling to room temperature after oxidation at 1400° C, reduces the strength at all temperatures. The strength drops to ~ 200 MN m^{-2} after ~ 20 min oxidation but does not exhibit any further decrease for oxidations of up to 24 h.

Finally, when the oxidised layer is removed by grinding, the strength attains a value similar to that of the unoxidised material.

5.3. Interpretation

The cracked surface layer must be responsible for the low strength of the oxidised material after cycling to room temperature, because removal of the cracks by grinding returns the strength to that of the unoxidised material. The stress to extend these cracks is given by equation 1, i.e. the equation for edge-cracks. The value of C is known, 15μm, but γ_i is not. Since the tips of the cracks are in material that has been only partially oxidised, however, it should not be very different from that for the silicon nitride itself. Using this γ_i-value, a crack-extension stress 200 MN m^{-2} is obtained, and this is similar to the observed strength.

The effects of oxidation on the strength of specimens cooled to temperatures above room temperature are more complex. Firstly, the temperature range corresponding to the sharp decrease in strength is equivalent to the temperatures at which cristobalite transforms from its high temperature to its low temperature form. This observation leaves little doubt that the cracks in the cristobalite, observed at room temperature, are created during the cristobalite transition at ~ 250° C. The strengths below the transition temperature are then determined by the stress to extend the cracks as described above.

The high strengths attained above the transition temperature require that the strength of the oxidised surface layer should be greater than the strength of the unoxidised nitride. However, the strength increase cannot be explained simply in terms of enhancement of the strength of the surface. If the internal pores were not affected by oxidation, they could propagate to fracture at a stress only $\sqrt{2}$ larger than the fracture stress of the unoxidised material – C in equation 1 is the semi-diameter of internal flaws but the overall diameter of surface flaws – whereas, the observed strengths between 300 and 600° C are in excess of this. Oxidation must therefore modify both internal and external flaws.

It remains to explain the progressive increase in strength, after oxidation, as the test temperature is reduced from 1400 to 300° C. The thermal expansion mismatch between the bulk material and the glazed layer could not give this increase because the mismatch is such that an increasing (but small) tensile stress is produced in the glaze as the temperature is lowered. Rather, the strength of oxidised material should reflect the strength of the oxide layer itself. The effect of temperature on the strength of cristobalite is not known but unlike Si_3N_4, most oxides show a strong temperature-dependence of strength at elevated temperatures [12, 18, 26, 27].

6. Conclusions

(i) The strength of reaction-sintered silicon nitride is determined by the stress to extend the largest pores. The main variables are E, γ_i and C.

(ii) For a given material, the strength varies little with temperature. This is an unusual feature, and is related both to the inability of the material to deform plastically, and the temperature-independence of γ_i.

(iii) High porosity leads to low strength because an increase in porosity reduces E and γ_i and increases C, all of which reduce strength.

(iv) For material of density, 2.55×10^3 kg m^{-3}, attention to fabrication conditions becomes important. The highest strengths are obtained by nitriding primarily below the silicon melting temperature, which minimises C.

(v) An enhancement of the strength of reaction-sintered silicon nitride can be achieved, in principle, by increasing Young's modulus and decreasing the size of the largest pores.

(vi) Oxidation at 1400° C produces cristobalite. Initially, the oxidation occurs around the pores

and the oxidation rate is rapid. Then, a dense surface layer develops which limits the subsequent supply of oxygen to the interior and reduces the oxidation rate. The cristobalite cracks on cooling below 250° C due to a phase transition. (vii) If the oxidised specimen is maintained above the phase transition temperature, the strength is enhanced. But below the transition temperature, the oxide layer cracks, which reduces the strength.

Acknowledgement

The authors wish to thank Messrs D. Gilling, R. N. C. Booth and P. Wilyman for fabricating the material and general experimental assistance. They are also indebted to Mr J. W. Henney and Mr R. W. M. Hawes for most valuable and illuminating discussions.

References

1. N. L. PARR and E. R. W. MAY, *Proc. Brit. Ceram. Soc.* 7 (1967) 81.
2. D. J. GODFREY, *Metals and Materials* (1968) 305.
3. D. E. STODDART and R. P. GRAHAM, *Materials Towards the 70's* (1969) 20.
4. P. GRIERSON, K. H. JACK, and S. WILD, Ministry of Defence Contract N/CP.61/9411/67/4B/MP.387, Progress Report No. 1, (1968).
5. P. L. PRATT, "Mechanical Properties of Engineering Ceramics", edited by W. W. Kriegel and H. Palmour (Interscience Publishers, New York, 1961) p. 507.
6. D. S. THOMPSON and P. L. PRATT, *Proc. Brit. Ceram. Soc.* **6** (1966) 37.
7. *Idem*, "Science of Ceramics", Vol. 3, edited by G. H. Stewart (Academic Press Inc., London, 1967) p. 33.
8. E. GLENNEY and T. A. TAYLOR, *Powder Metallurgy* **1-2** (1958) 189.
9. D. E. LLOYD, "Special Ceramics", Vol. 4, edited by P. Popper (Academic Press Inc., London, 1968) p. 165
10. G. C. DEELEY, J. M. HERBERT, and N. C. MOORE, *Powder Metallurgy* **8** (1961) 145.
11. N. L. PARR, R. SANDS, P. L. PRATT, E. R. W. MAY, C. R. SHAKESPEARE, and D. S. THOMPSON, *ibid* 145.
12. A. G. EVANS and R. W. DAVIDGE, *J. Nucl. Mt.* **33** (1969) 249.
13. R. W. DAVIDGE and G. TAPPIN, *J. Mater. Sci.* **3** (1968) 165.
14. A. G. EVANS and R. W. DAVIDGE, *Phil. Mag.* **20** (1969) 373.
15. R. W. DAVIDGE and G. TAPPIN, *Proc. Brit. Ceram. Soc.* **15** (1970) in press.
16. T. R. WILSHAW, private communication.
17. W. F. BROWN and J. E. SRAWLEY (ASTM 1967) STP 410, p.13.
18. A. G. EVANS, D. GILLING, and R. W. DAVIDGE, *J. Mater. Sci.* **5** (1970) 187.
19. D. M. MARSH, *Proc. Roy. Soc.* **A279** (1964) 420.
20. A. S. TETELMAN and A. J. MCEVILY, "Fracture of Structural Materials" (John Wiley and Sons Inc., New York, 1967) p. 64.
21. R. A. SACK, *Proc. Phys. Soc.* **58** (1946) 729.
22. R. W. DAVIDGE, unpublished data.
23. R. J. LUMBY and R. F. COE, *Proc. Brit. Ceram. Soc.* **15** (1970) in press.
24. U. R. EVANS, "The Corrosion and Oxidation of Metals", First Supplementary Vol. (Arnold, London, 1968).
25. W. D. KINGERY, "Introduction to Ceramics" (John Wiley and Sons Inc, New York, 1960) 483.
26. B. A. PROCTOR, I. WHITNEY, and J. W. JOHNSON, *Proc. Roy. Soc.* **A297** (1967) 534.
27. R. M. SPRIGGS, J. B. MITCHELL, and T. VASILOS, *J. Amer. Ceram. Soc.* **47** (1964) 323.

Received 22 December 1969 and accepted 16 January 1970